Available online at www.sciencedirect.com

SciVerse ScienceDirect

Ceramics International 39 (2013) 7119–7126

CERAMICS INTERNATIONAL

www.elsevier.com/locate/ceramint

Silver-loaded TiO_2 powders prepared through mechanical ball milling

Basak Aysin[a], Abdullah Ozturk[a], Jongee Park[b,*]

[a]Department of Metallurgical and Materials Engineering, Middle East Technical University, Ankara 06531, Turkey
[b]Department of Metallurgical and Materials Engineering, Atilim University, Ankara 06836, Turkey

Received 22 January 2013; received in revised form 16 February 2013; accepted 17 February 2013
Available online 26 February 2013

Abstract

Silver (Ag) was loaded on TiO_2 powders through mechanical ball milling. Ag-loading was accomplished by adding 4.6, 9.2, and 13.8 ml of $AgNO_3$ solution to the TiO_2 powders during the milling process. The resulting powder was characterized by XRD, XPS, SEM, and EDS. The photocatalytic activity of the silver-loaded powder was evaluated in terms of the degradation of methyl orange (MO) solution under ultraviolet (UV) illumination. XRD patterns were refined using the Rietveld analysis to determine the lattice parameters. XRD analysis suggested that Ag was loaded on TiO_2 powders in the form of AgO. X-ray photoelectron spectroscopy and Rietveld analysis revealed that silver did not dope into the crystal structure of TiO_2. SEM investigations confirmed that ball milling caused a decrease in the average particle size of the powders. Silver-loading improved the photocatalytic activity of the TiO_2 powders. The TiO_2 powder ball milled without Ag-loading degraded 46% of the MO solution whereas the ball milled with 13.8 ml $AgNO_3$ solution degraded 96% of the MO solution under 1 h UV irradiation. Moreover, TiO_2 powders gained antibacterial property after Ag-loading.

Keywords: D. TiO_2; Silver; Mechanical ball milling; Photocatalysis

1. Introduction

Titanium dioxide, TiO_2, has been used widely as a photocatalyst due to its relatively high photocatalytic activity, biological and chemical stability, low cost, non-toxicity, and long stable life [1–5]. The photocatalyst TiO_2 generates an extremely strong oxidizing power that oxides harmful substances and eliminates them by decomposition into carbon dioxide, water and other small molecules when it is exposed to a light source [3–7]. However, TiO_2 photocatalyst is effective only under UV light ($\lambda < 388$ nm) irradiation due to its large energy band gap (i.e. 3.2 eV for anatase). In addition, a high degree of electron–hole recombination results in low photoquantum efficiency, which severely limits the practical applications of TiO_2 as a photocatalyst although it has been investigated for over two decades [8–10]. Therefore, basic research and industrial development of high-efficiency TiO_2 photocatalyst are still attractive topics due to its industrial importance. Several investigations have been done to improve the photocatalytic efficiency of TiO_2 since the discovery of photocatalysis by Fujishima in the early 1970s [6]. In that regard, different production techniques such as sol–gel processing, hydrothermal processing, ball milling [11–13], or different modifications, such as doping with a metal and a non-metal, co-doping with a metal and non-metal [14–16], or coupling with other semiconductors [17] have been tried.

Silver is most suitable for industrial applications due to its inexpensiveness and easy preparation. The Ag-loaded TiO_2 has a high Schottky barrier and acts as electron traps, facilitating electron–hole separation and promoting the interfacial electron transfer process [10]. Under UV-light irradiation, the photogenerated electrons quickly transfer from the TiO_2 surface to the Ag particles and result in the improvement of photocatalytic efficiency. Various methods, such as photochemical deposition [18], chemical reduction method [19], hydrothermal method [20], sol–gel process [21,22], and laser induction [23], have been

*Corresponding author. Tel.: +90 312 586 8786; fax: +90 312 586 8091.
E-mail address: jpark@atilim.edu.tr (J. Park).

0272-8842/$ - see front matter © 2013 Elsevier Ltd and Techna Group S.r.l. All rights reserved.
http://dx.doi.org/10.1016/j.ceramint.2013.02.054

explored to load silver onto TiO_2. However, Ag doping on TiO_2 particles by mechanical ball milling has not been the subject of any scientific study until now. Therefore, it has both scientific and technological significance.

The purpose of this study was to prepare Ag-loaded TiO_2 powder through mechanical ball milling, and also to produce a TiO_2 powder with photocatalytic properties comparable to a photocatalyst TiO_2 powder (P-25). The powders prepared were characterized using XRD, SEM, EDS, and XPS analysis techniques. The photocatalytic activity of the powders was evaluated in terms of the degradation of methylene orange (MO) solution under UV-light illumination. Likewise, the antibacterial activity of the Ag-loaded TiO_2 particles was investigated.

2. Experimental

2.1. Powder preparation

The process was initialized by using anatase TiO_2 (NT-22) purchased from Nano Co. All other chemicals used in this study were of analytical grade and used in the as-received form, without further purification. The NT-22 powders in as-received form and in ball-milled form without the addition of $AgNO_3$ solution were coded N and N0, respectively. The NT-22 powder ball milled with the addition of $AgNO_3$ solution was named Ag-loaded TiO_2 powder. Three different Ag-loaded TiO_2 powders produced by ball milling the starting powder with 4.6, 9.2 and 13.8 ml of 0.1 M $AgNO_3$ solution were coded N1, N2, and N3, respectively. Hereafter, the powders will be referred to by their codes unless otherwise mentioned.

Ag-loaded TiO_2 powders were prepared by adapting the procedure described by Kondo and Jardim [24]. First, an $AgNO_3$ (Merck) solution of 0.1 M and a Na_2CO_3 (Horasan Kimya) solution of 1% weight/volume (w/v) were prepared separately. Then, 10 g of TiO_2 powder was poured into a 250 ml zirconia jar containing 50 ml of distilled water. An $AgNO_3$ solution of 4.6 ml and a Na_2CO_3 solution of 5 ml were then added into the zirconia jar. After that, 2 ml of dispersant (Darvan C-N, Vanderbilt Co.) and 200 g of zirconia balls with a 5 mm diameter were added into the jar. Finally, the jar was fastened to a planetary ball mill (PM-100, Retsch). Milling was performed at 200 rpm for 1 h continuously without any interval breaks.

After milling, the suspension was taken out of the jar and poured into a glass beaker. Then, the beaker was placed in a dryer at 100 °C for 4 h. After drying was completed, agglomerated powders were ground gently using an agate mortar and pestle. After that, the ground powders were calcined at 400 °C for 1 h to remove any organic compounds and to allow the diffusion of Ag into the TiO_2. The procedure was repeated for 9.2 ml $AgNO_3$ and 10 ml Na_2CO_3 solutions as well as for 13.8 ml $AgNO_3$ and 15 ml Na_2CO_3 solutions to observe the effects of increasing amounts of $AgNO_3$ solution on the Ag-loading process.

2.2. Characterization

Powder XRD technique was employed to identify the phases present in the TiO_2 powders. The XRD patterns of the TiO_2 powders were taken with Cu target Kα radiation by using a Rigaku Geiger-Flex DMAK/B model diffractometer. Each powder was scanned from 2θ of 20–80° at a rate of $2^\circ\,min^{-1}$ by 0.02° increments continuously. Crystallite size was calculated by applying the Debye–Scherrer formula on the characteristic peaks of the TiO_2 powders. For crystallite size calculations, the characteristic peak of each powder was scanned at a rate of $0.5^\circ\,min^{-1}$ by 0.02° increment. The changes in the lattice parameters of the powders were calculated and evaluated using UnitCell [11].

An X-ray photoelectron spectroscope (XPS) was employed with Al Kα radiation to investigate the surface composition and chemical states of the powders. Detailed scans were recorded for Ti 2p and Ag 3d. Doped atoms at the surface of TiO_2 were analyzed by means of binding energies obtained from XPS.

A scanning electron microscope (Nova NANOSEM 430) was employed to examine surface morphology and particle size of the TiO_2 powders. Elemental analysis was performed to detect the presence and percentage of Ag in the powders. The specific surface area of the powders was measured using an Autosorb-6 apparatus (Quantachrome Co.) by multi-point Brunauer, Emmett and Teller (BET) method.

2.3. Photocatalytic activity measurements

Photocatalytic activity measurements were carried out in a homemade enclosed box, which provided a fully dark environment without allowing light exposure within the box. A Black-Ray-grade UV semiconductor inspection lamp (100 W, 230 V ~50 Hz, 2.0 A, 365 nm) and a magnetic stirrer were present inside the box. A UV–vis single beam spectrophotometer (Scinco, S-3100) was used for the photocatalytic activity measurements. A 10 mg/L of Methyl Orange (MO) solution was prepared by dissolving MO powder (Fluka) in de-ionized water. A 0.1 g TiO_2 powder was added into a 100 ml of MO solution and the suspension was stirred continuously at 500 rpm by a magnetic stirrer in the dark for 30 min for the powders to absorb the MO solution and reach absorption–desorption equilibrium. At the end of the first 30 min, a sample of 3.5 ml was taken from the suspension by means of syringe filters (Millex Millipore, 0.22 μm) for spectrophotometer measurement. After the first measurement, the UV lamp was turned on and changes in absorbance under UV light were measured after 30 and 60 min. The photocatalytic activity of a well-known TiO_2 photocatalyst, P-25 powder (Degussa), was also measured in the same test conditions for comparison purposes.

2.4. Antibacterial activity test

The suspension taken from the ball mill was spin-coated on glass substrates for 30 s. After coating, the substrate was dried at 180 °C for 5 min. This process was repeated five times for each powder suspension to obtain a homogeneous and appropriate coating on the substrate. Coated sides of glass substrates were placed into agar plates containing *E. coli* bacteria. Then the plates were incubated at 37 °C for 48 h. Bare glass substrate and P-25-powder-coated glass substrate were also placed into agar plates as control specimens. The photographs of the inhibition zones of the substrates were taken for the comparison of antibacterial activity for each specimen.

3. Results and discussion

The XRD patterns of all powders possess the characteristic (101) diffraction peak of anatase TiO_2 at 2θ of $\sim$25.3° (JCPDS #21-1272) as shown in Fig. 1. In addition to the peaks diffracted from anatase TiO_2, a small but visible diffraction peak of AgO (-111) at 2θ of $\sim$32.3° (JCPDS #89-3081) was detected in the patterns of the powders N2 and N3. AgO was not identified in the XRD pattern of the N1 powder due to the fact that the low AgO peak was indistinguishable from the background. The intensity of the AgO peak increased slightly when the $AgNO_3$ addition during ball milling was increased as best seen in the inset in Fig. 1. Again, the characteristic (111) diffraction peak of AgO is unseen in the patterns since it overlaps with (103) the peak of the anatase phase at 2θ of $\sim$37.04°. The characteristic (110) diffraction peak of rutile TiO_2 at 2θ of $\sim$27.4° (JCPDS #21-1276) is absent in all patterns. The XRD analysis suggests that only anatase TiO_2 is present and rutile TiO_2 does not exist in all the powders both before and after Ag-loading by ball milling. In addition, no phase change was recognized in the TiO_2 powders after Ag-loading followed by calcination. The occurrence of the characteristic (101) diffraction peak of anatase TiO_2 at nearly the same diffraction angles after Ag-loading implies that Ag did not dope into the crystal lattice of TiO_2.

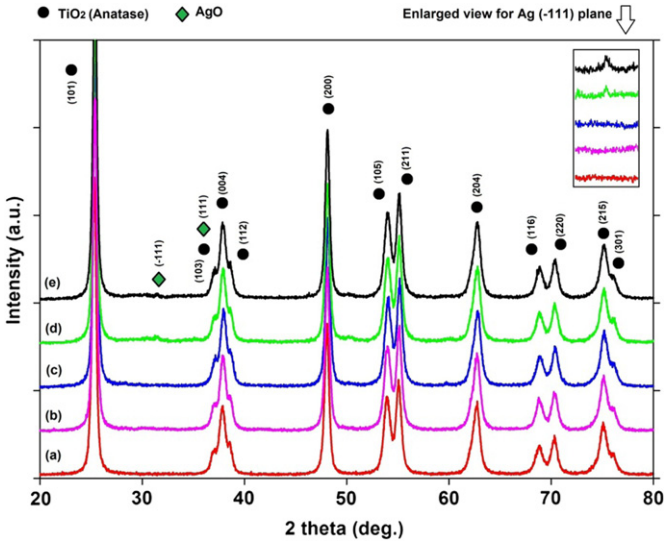

Fig. 1. XRD patterns of the (a) N, (b) N0, (c) N1, (d) N2, and (e) N3 powders.

The values calculated for the lattice parameters, crystallite volume and crystallite size for the powders are given in Table 1. The lattice parameters and crystallite size for the powders agree well with those given in the JCPDS card of the anatase phase. The lattice parameter "*a*" remained more or less the same, around 3.78 Å, after milling as well as after Ag-loading. Nevertheless, a small change in the "*c*" parameter was observed after milling and Ag-loading. A noticeable change in the lattice parameters is the result of plastic deformation, leading to lattice distortion [25]. For all powders after the milling process, crystallite size was about the same (22.18 nm), which is slightly smaller than the size of the starting powder (22.6 nm). The decrease in crystallite size may be due to the production of O vacancies in TiO_2. No significant change in the cell volume of the powders led to the conclusion that Ag did not dope into the TiO_2 lattice.

The surface morphology of all powders is shown in the SEM images in Fig. 2. SEM analysis revealed that the TiO_2 particles in all powders are irregular in shape and rather agglomerated, and AgO is either dispersed on the surface of TiO_2 particles or between the interfaces of TiO_2 agglomerates. The surface morphology and shapes of particles did not change after ball milling and Ag-loading. The particles in the milled and Ag-loaded powders seem more agglomerated than the ones in powder N. The particle size of the powders, as measured from the SEM images, is shown in Table 2.

As seen in Fig. 2, the particle size of powder N is around 80–90 nm. The manufacturer of this powder quoted particle size as 15–30 nm. Particle size data obtained from the SEM images may not be true because of the agglomeration, but they have been measured for comparison of the size of particles before and after ball milling and Ag-loading. The particle size of the powders decreased after only ball milling without Ag-loading. However, the particle size of the Ag-loaded powders increased with Ag-loading. The increase in particle size of the Ag-loaded powders was related to agglomeration induced by both ball milling and AgO coating onto the surface of the TiO_2 particles [26]. The mechanical energy accelerated the

Table 1
The lattice parameters and crystallite size of the powders.

Parameter	Powder				
	N	N0	N1	N2	N3
a (Å)	3.7850	3.7818	3.7835	3.7822	3.7832
c (Å)	9.5098	9.5189	9.4993	9.5098	9.4996
Crystallite volume ($Å^3$)	136.2395	136.1394	135.9813	136.0380	135.9640
Crystallite size (nm)	22.63	22.17	22.22	22.19	22.13

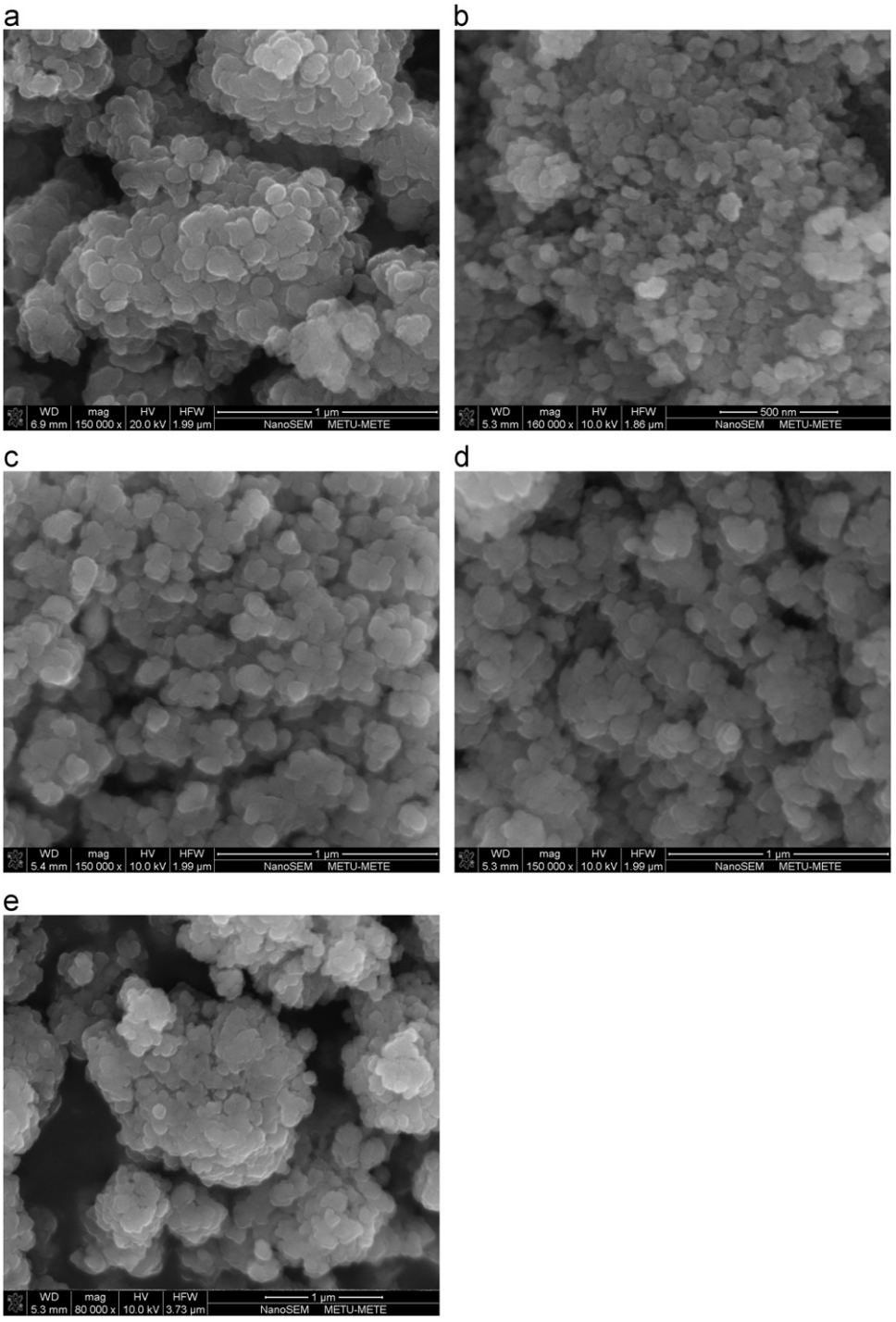

Fig. 2. SEM images of the (a) N, (b) N0, (c) N1, (d) N2, and (e) N3 powders.

Table 2
SEM particle size and BET specific surface area of the powders.

Property	Powder				
	N	N0	N1	N2	N3
SEM particle size (nm)	88.8	82.6	85.5	92.8	98.9
BET specific surface area (m^2/g)	78.53	81.64	71.38	71.22	64.89

aggregation because the fresh surfaces exposed by the milling process lowered their high surface energy by agglomeration [27].

The specific surface area of the powders is presented in Table 2. The measured specific surface area of powder N was 78.53 m^2/g, which was in agreement with the value (60–80 m^2/g) reported by the manufacturer of this powder. The specific surface area for powder N0 was a little larger than the starting

powder, indicating that particle refinement was efficient as a result of ball milling. After Ag-loading, the specific surface area of TiO_2 particles decreased. A large specific surface area is desirable since a large amount of absorbed organic molecules on the surface can promote the photocatalytic reaction. Therefore, a large specific surface area provides more absorbing sites for reactant MO molecules. The lowest value (64.89 m^2/g) for the specific surface area was obtained for powder N3. The decrease in specific surface area after Ag-loading was also reported by Iliev et al. [28] and Kondo and Jardim [24] and may be related to the increase in particle size due to Ag-coating [26] or due to the blocking of fine capillaries on the parent TiO_2 surface by metal film islands [29,30]. It has also been noted that BET-specific surface area data of the powders were compatible with the particle size data.

The elemental composition of the powders in weight percentage as obtained from the EDS analysis is given in Table 3. As expected, Ag concentration in the powders increased as the amount of the $AgNO_3$ solution added to the starting powder during ball milling was increased.

The fully scanned XPS spectra for N and N3 powders are shown in Fig. 3. The Ag 3d peaks are clearly seen in the spectrum of the N3 powder. Two peaks located at 458.4 eV and 464.1 eV were identified as Ti $2p_{3/2}$ and Ti $2p_{1/2}$ of TiO_2, respectively. The XPS analysis revealed that the presence of Ag exerts no significant influence on the XPS spectra in either the Ti 2p level or the O 1s level.

Table 3
Elemental composition of the powders.

Element	Powder				
	N	N0	N1	N2	N3
O K	48.36	48.81	48.78	49.70	56.56
Ag L	0	0	0.49	0.69	0.91
Ti K	51.64	51.19	50.73	49.61	42.53

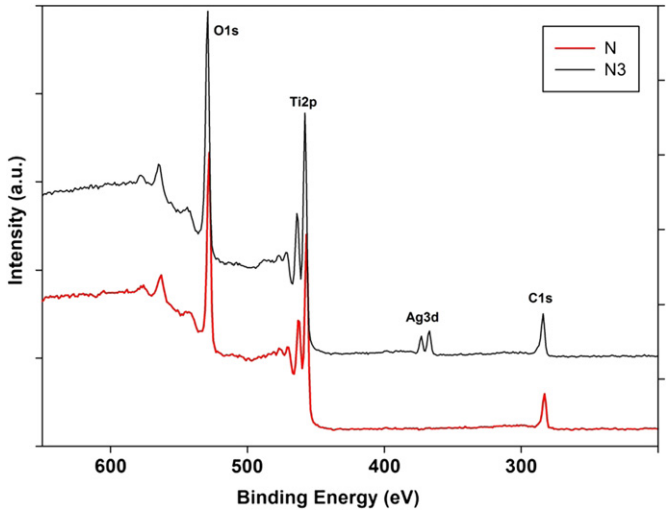

Fig. 3. XPS survey spectra for powders N and N3.

For a closer inspection, the XPS spectra of the N3 powder between 362 and 372 eV is shown in Fig. 4. The data was fitted according to the Lorentzian peak shape and calibrated according to C1s peak. Ag $3d_{5/2}$ peak detected at 367.1 eV is attributed to the presence of AgO [31] implying that Ag is present in the form of AgO. The XPS results are concomitant with the XRD results and provide the evidence that Ag do not enter TiO_2 lattice but exists as an individual phase in N3.

The peaks for Ti between 450 and 468 eV shown in Fig. 5 were also fitted and calibrated like the ones for Ag. Any remarkable shift could not be detected after Ag-loading. Therefore, it is concluded that Ag did not weave into the TiO_2 lattice structure and remained as AgO over the TiO_2 particles [32].

Degussa P-25 TiO_2 powder was taken as the reference photocatalyst to compare the photocatalytic performance of the prepared powders. Fig. 6 shows the degradation of the MO solution with respect to the irradiation time for all the powders. Without UV irradiation, all the powders did not

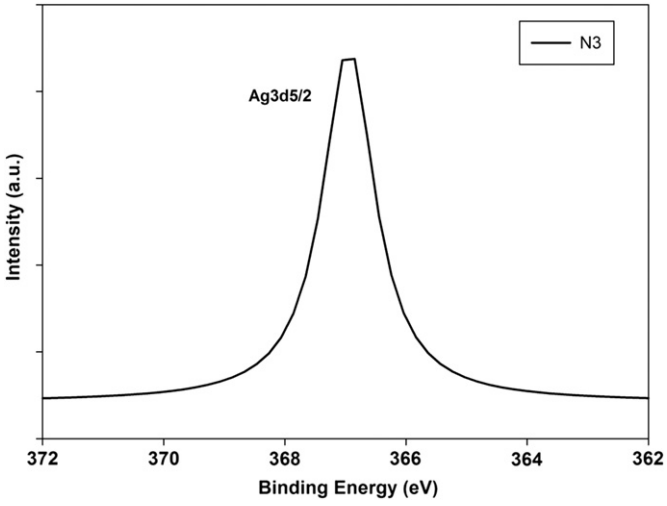

Fig. 4. The XPS spectra of Ag $3d_{5/2}$ for powder N3.

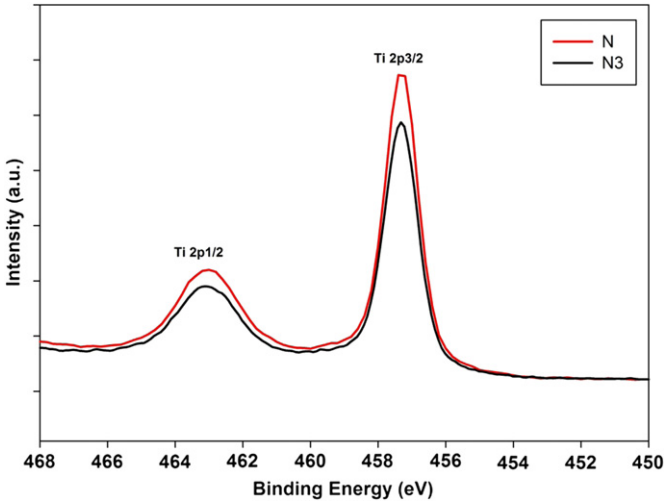

Fig. 5. XPS spectra of Ti 2p for powders N and N3.

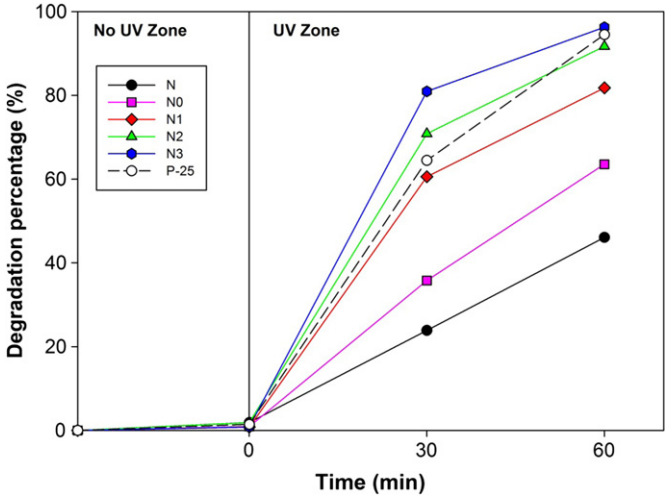

Fig. 6. Variation of MO degradation with irradiation time for all of the powders investigated.

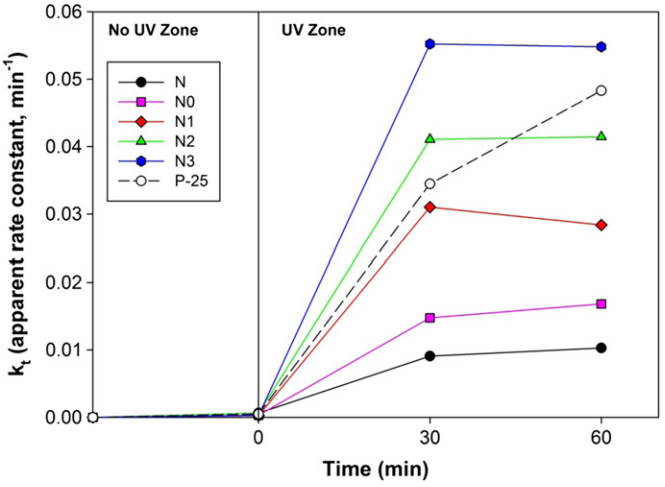

Fig. 7. Variation of the reaction rate of MO degradation with irradiation time for all of the powders investigated.

provide any noteworthy degradation of MO. All MO degradation was caused by photocatalytic reaction only. N3 powder gave the best result in terms of MO degradation. N3 and P-25 powders decomposed 96.3% and 94.5% of the MO in 60 min of UV irradiation, respectively. Results revealed that as the Ag-loading increased, the photocatalytic activity of the powder increased as well due to Ag acting as electron traps to enhance the electron–hole separation. Moreover, Ag also enhanced the transfer of trapped electrons to the absorbed O_2 acting as an electron acceptor [33]. Ball milling without Ag-loading increased the photocatalytic activity due to the increase of the specific surface area.

Fig. 7 shows the variation of the apparent rate constant with the irradiation time for all the powders investigated. The reaction rate of MO degradation increased in the first 30 min for all the powders. N3 powder had the highest reaction rate in terms of MO degradation in the first 30 min of UV irradiation time. After the first 30 min, the reaction rate of powders N, N0, and P-25 continued to increase but that of powders N1, N2, and N3 decreased, implying that Ag-loaded powders reached the maximum rate within 30 min of UV irradiation. However, powder N3 still had the highest reaction rate in terms of MO degradation at the end of 60 min of UV irradiation time.

The enhanced activity of Ag-loading is attributed to the particle size reduction, high anatase crystallinity, large amount of surface oxygen vacancy, intense light absorption, and narrow band gap. The possible reason why Ag-loaded TiO_2 exhibited a better photocatalytic activity for the degradation of MO under UV irradiation could be explained using the scheme shown in Fig. 8. When two materials having different work functions, such as TiO_2 and Ag, contact each other, formation of a Schottky barrier is observed. Electrons will be transferred from the material with low work function (TiO_2) to the material with high work function (Ag), facilitating electron transfer from TiO_2 to Ag. The electrons transferred and loaded on the surface of

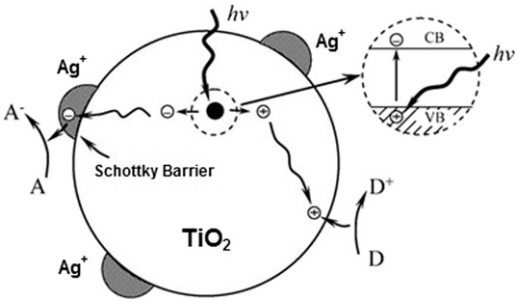

Fig. 8. Schematic illustration of the photocatalysis mechanism of Ag-loaded TiO_2.

Ag will be scavenged by the electron acceptor, commonly the oxygen molecules absorbed on the Ag surface. It is possible for the photogenerated electrons at the conduction band to fall onto the doping energy level of the Ag species. The photogenerated electrons are transferred from the conduction band to the surface and then captured by the absorbed O_2, thereby enhancing the separation efficiency of the photogenerated charge carriers. Moreover, some electrons that are transferred to Ag are contained in the body of the TiO_2 and electron–hole recombination rate is decreased by the transfer of electrons. Ag atoms act as electron traps, capturing certain amounts of photoelectrons produced by UV excitation. This way, the separation between the photoelectron and the hole is increased. In addition, Ag-loading increases the quantity of photogenerated charge carriers compared to unloaded TiO_2. As a result, more departed photogenerated electrons and holes (h^+/e^-) participate in the photodegradation process, resulting in higher photocatalytic efficiency.

Ag was detected as AgO in the Ag-loaded powders by XRD and XPS analyses. SEM investigation revealed that AgO is coated on the surface of the TiO_2 particles. The reaction mechanism of the Ag-loaded TiO_2 could be interpreted as follows: In principle, UV illumination can convert AgO to the native metal in the presence of TiO_2 [34]. AgO can be photodecomposed into O and Ag

according to the following reaction [35]:

$$AgO \xrightarrow{\lambda} Ag + \tfrac{1}{2}O_2$$

Similarly, upon exposure of Ag–TiO_2 to UV irradiation, electron and holes are generated

$$Ag\text{-}TiO_2 \xrightarrow{\lambda} e^-_{cb} + h^+_{vb}$$

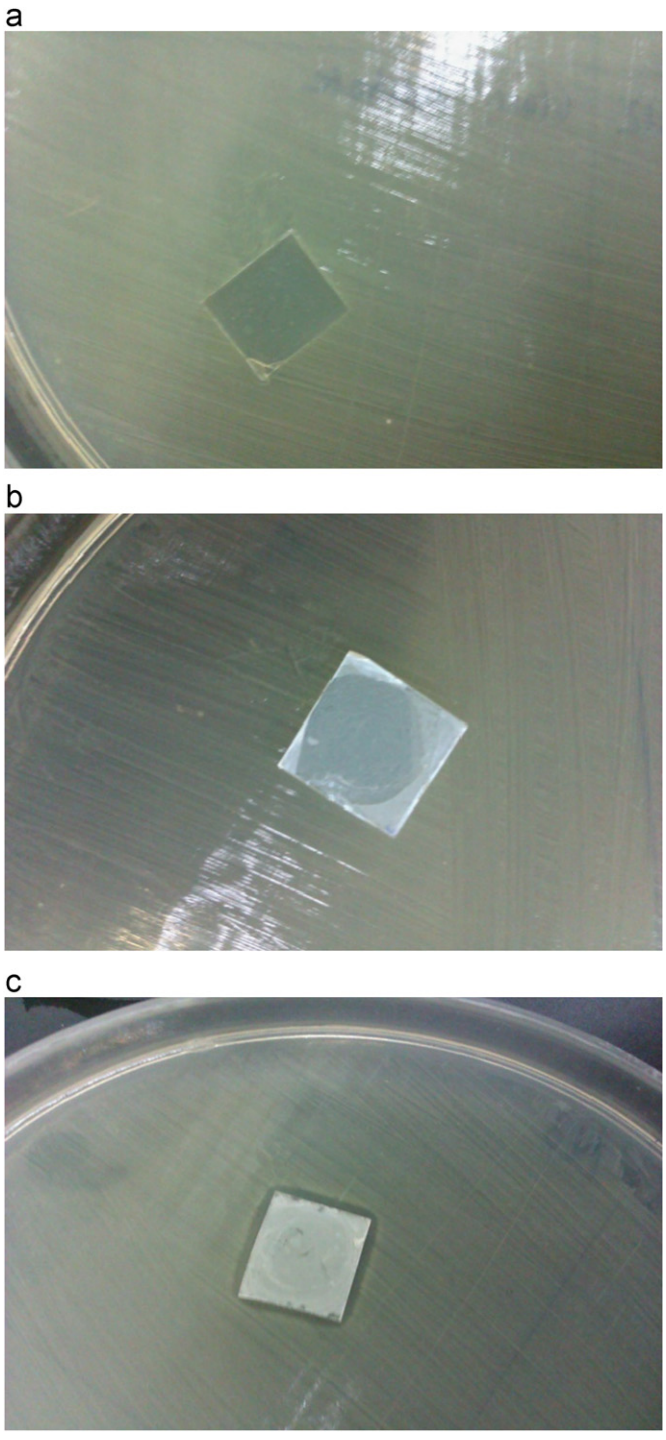

Fig. 9. Photographs of glass substrates in agar plates with *E. coli*: (a) No powder, (b) powder N, and (c) powder N3.

The Ag on the surface of the TiO_2 can be generated to Ag^+ ion by holes

$$Ag_s + h^+_{vb} \rightarrow Ag^+_s$$

Ag^+ ions trap the electrons.

$$Ag^+_s + e^- \rightarrow Ag_s$$

The photogenerated holes oxidized the preabsorbed OH^- and H_2O to generate $^{\bullet}HO$ free radicals, which react with absorbed MO [36].

$$OH^-_s + h^+_{vb} \rightarrow {}^{\bullet}OH$$

$$H_2O_s + h^+_{vb} \rightarrow {}^{\bullet}OH + H^+$$

$$OH + MO \rightarrow \text{colorless product}$$

The subscripts vb, cb, and s represent valence band, conductive band, and surface of catalyst, respectively.

The photographs of substrates in the agar plates after incubation at 37 °C for 48 h are shown in Fig. 9. Bare glass substrate and the substrate coated with powder N did not show any antibacterial activity. When the substrate coated with N3 powder was examined, a bacterial free zone around the glass substrate was observed, which indicates antibacterial activity [37]. The antibacterial mechanism depends on the attack to the cell membrane of the bacteria [26]. During UV irradiation of the TiO_2, hydroxyl radicals are formed. These radicals can attack effectively the cell membrane of the bacteria and break them down [37]. In the case of Ag, Ag^+ ions are the attacking agents, but it is noted that Ag in oxide form shows antibacterial activity whether a light source is present or not while Ag^+ does not have any activity if the light is absent [34].

4. Conclusions

The silver-loaded photocatalyst TiO_2 can be successfully prepared by mechanical ball milling. The mechanical milling causes a coupling reaction and change in the surface morphology of TiO_2. During the milling, Ag atoms may not dope into the lattice structure but remain on the surface of the TiO_2 particle. The loaded silver is highly dispersed and present in AgO form. The Ag-loading increases the quantity of photogenerated charge carriers which participate in the photodegradation process and results in higher photocatalytic activity. Even with a small amount of Ag-loading, the photocatalytic degradation rate of the MO solution on TiO_2 powder can be greatly improved. Compared with unloaded TiO_2 powder, Ag-loaded TiO_2 powder shows a 50% enhancement in photocatalytic degradation of MO solution under 1 h UV-light illumination. Moreover, the prepared Ag-doped TiO_2 powder has antibaterial properties when a light source is given.

Acknowledgments

Authors gratefully acknowledge the partial financial support of the Scientific and Technological Council of Turkey (TUBİTAK) through the Project no. 109M048.

References

[1] A. Fujishima, X. Zhang, Titanium dioxide photocatalysis: present situation and future approaches, Comptes Rendus Chimie 9 (2006) 750–760.
[2] U. Diebold, The surface science of titanium dioxide, Surface Science Reports 48 (2003) 53–229.
[3] T. Zhang, T. Oyama, S. Horikoshi, J. Zhao, H. Hidaka, Photocatalytic decomposition of the sodium dodecylbenzene sulfonate surfactant in aqueous titania suspensions exposed to highly concentrated solar radiation and effects of additives, Applied Catalysis B: Environmental 42 (2003) 13–24.
[4] N. San, A. Hatipoglu, G. Kocturk, Z. Cinar, Photocatalytic degradation of 4-nitrophenol in aqueous TiO_2 suspensions: theoretical prediction of the intermediates, Journal of Photochemistry and Photobiology A: Chemistry 146 (2002) 189–197.
[5] J. Park, Photocatalytic activity of hydroxyapatite-precipitated potassium titanate whiskers, Journal of Alloys and Compounds 492 (2010) 57–60.
[6] A. Fujishima, T.N. Rao, D.A. Tryk, Titanium dioxide photocatalysis, Journal of Photochemistry and Photobiology C: Photochemistry Reviews 1 (2000) 1–21.
[7] O. Carp, C.L. Huisman, A. Reller, Photoinduced reactivity of titanium dioxide, Progress in Solid State Chemistry 32 (2004) 33–177.
[8] T. Umebayashi, T. Yamaki, H. Itoh, K. Asai, Band gap narrowing of titanium dioxide by sulfur doping, Applied Physics Letters 81 (2002) 454–456.
[9] Y. Ishibai, J. Sato, S. Akita, T. Nishikawa, S. Miyagishi, Photocatalytic oxidation of NO_x by Pt-modified TiO_2 under visible light irradiation, Journal of Photochemistry and Photobiology A: Chemistry 188 (2007) 106–111.
[10] B. Xin, Z. Ren, H. Hu, X. Zhang, C. Dong, K. Shi, L. Jing, H. Fu, Photocatalytic activity and interfacial carrier transfer of Ag–TiO_2 nanoparticle films, Applied Surface Science 252 (2005) 2050–2055.
[11] D.H. Kim, H. Hong, S. Kim, J. Song, K. Lee, Photocatalytic behaviors and structural characterization of nanocrystalline Fe-doped TiO_2 synthesized by mechanical alloying, Journal of Alloys and Compounds 375 (2004) 259–264.
[12] D.H. Kim, K.S. Lee, Y.-S. Kim, Y.-C. Chung, S.-J. Kim, Photocatalytic activity of Ni 8 wt%-doped TiO_2 photocatalyst synthesized by mechanical alloying under visible light, Journal of the American Ceramic Society 89 (2006) 515–518.
[13] J. Ovenstone, Preparation of novel titania photocatalysts with high activity, Journal of Materials Science 36 (2001) 1325–1329.
[14] A. Zaleska, Doped-TiO_2: a review, Recent Patents on Engineering 2 (2008) 157–164.
[15] H. Tian, J. Ma, K. Li, J. Li, Hydrothermal synthesis of S-doped TiO_2 nanoparticles and their photocatalytic ability for degradation of methyl orange, Ceramics International 35 (2009) 1289–1292.
[16] B. Babić, J. Gulicovski, Z. Dohčević-Mitrović, D. Bučevac, M. Prekajski, J. Zagorac, B. Matović, Synthesis and characterization of Fe^{3+} doped titanium dioxide nanopowders, Ceramics International 38 (2012) 635–640.
[17] S.G. Kumar, L.G. Devi, Review on modified TiO_2 photocatalysis under UV/visible light: selected results and related mechanisms on interfacial charge carrier transfer dynamics, The Journal of Physical Chemistry A 115 (2011) 13211–13241.
[18] W. Lee, H.-S. Shen, K. Dwight, A. Wold, Effect of silver on the photocatalytic activity of TiO_2, Journal of Solid State Chemistry 106 (1993) 288–294.
[19] R. Priya, K.V. Baiju, S. Shukla, S. Biju, M.L.P. Reddy, K. Patil, K.G.K. Warrier, Comparing ultraviolet and chemical reduction techniques for enhancing photocatalytic activity of silver oxide/silver deposited nanocrystalline anatase titania, The Journal of Physical Chemistry C 113 (2009) 6243–6255.
[20] Y. Liu, C.-Y. Liu, Q.-H. Rong, Z. Zhang, Characteristics of the silver-doped TiO_2 nanoparticles, Applied Surface Science 220 (2003) 7–11.
[21] B.A. Akgun, C. Durucan, N.P. Mellott, Effect of silver incorporation on crystallization and microstructural properties of sol–gel derived titania thin films on glass, Journal of Sol–Gel Science and Technology 58 (2011) 277–289.
[22] F. Ghanbary, A. Jafarian, Preparation and photocatalytic properties of silver doped titanium dioxide nanoparticles and using artificial neural network for modeling photocatalytic activity, Journal of Applied Sciences Research 5 (2011) 2193–2202.
[23] T.-jen Whang, H.-yu Huang, M.-tao Hsieh, J.-jen Chen, Laser-induced silver nanoparticles on titanium oxide for photocatalytic degradation of methylene blue, International Journal of Molecular Sciences 10 (2009) 4707–4718.
[24] M.M. Kondo, W.F. Jardim, Photodegradation of chloroform and urea using Ag-loaded titanium dioxide as catalyst, Water Research 25 (1991) 823–827.
[25] C. Shifu, Z. Wei, L. Wei, Z. Sujuan, Preparation, characterization and activity evaluation of p–n junction photocatalyst p-ZnO/n-TiO_2, Applied Surface Science 255 (2008) 2478–2484.
[26] J. Keleher, J. Bashant, N. Heldt, L. Johnson, Y. Li, Photo-catalytic preparation of silver-coated TiO_2 particles for antibacterial applications, World Journal of Microbiology and Biotechnology 18 (2002) 133–139.
[27] C. Suryanarayana, Mechanical alloying and milling, Progress in Materials Science 46 (2001) 1–184.
[28] V. Iliev, D. Tomova, L. Bilyarska, A. Eliyas, L. Petrov, Photocatalytic properties of TiO_2 modified with platinum and silver nanoparticles in the degradation of oxalic acid in aqueous solution, Applied Catalysis B: Environmental 63 (2006) 266–271.
[29] S. Sakthivel, M.V. Shankar, M. Palanichamy, B. Arabindoo, D.W. Bahnemann, V. Murugesan, Enhancement of photocatalytic activity by metal deposition: characterisation and photonic efficiency of Pt, Au and Pd deposited on TiO_2 catalyst, Water Research 38 (2004) 3001–3008.
[30] N. Sobana, M. Muruganadham, M. Swaminathan, Nano-Ag particles doped TiO_2 for efficient photodegradation of direct azo dyes, Journal of Molecular Catalysis A–Chemical 258 (2006) 124–132.
[31] B. Xin, L. Jing, Z. Ren, B. Wang, H. Fu, Effects of simultaneously doped and deposited Ag on the photocatalytic activity and surface states of TiO_2, The Journal of Physical Chemistry B 109 (2004) 2805–2809.
[32] L. Wen, B. Liu, X. Zhao, K. Nakata, T. Murakami, A. Fujishima, Synthesis, characterization, and photocatalysis of Fe-doped TiO_2: a combined experimental and theoretical study, International Journal of Photoenergy 2012 (2012) (Article ID 368750).
[33] H.M. Sung-suh, J.R. Choi, H.J. Hah, S.M. Koo, Y.C. Bae, Comparison of Ag deposition effects on the photocatalytic activity of nanoparticulate TiO_2 under visible and UV light irradiation, Journal of Photochemistry and Photobiology A: Chemistry 163 (2004) 37–44.
[34] K. Page, R.G. Palgrave, I.P. Parkin, M. Wilson, L.P. Savin, A.V. Chadwick, Titania and silver–titania composite films on glass-potent antimicrobial coatings, Journal of Materials Chemistry 17 (2007) 95–104.
[35] B. Ohtani, S.-W. Zhang, T. Ogita, S. Nishimoto, T. Kagiya, Photoactivation of silver loaded on titanium (IV) temperature decomposition of ozone, Journal of Photochemistry and Photobiology A: Chemistry 71 (1993) 195–198.
[36] L. Chen, T.-chuan Chou, Photodecolorization of methyl orange using silver ion modified TiO_2 as photocatalyst, Industrial and Engineering Chemistry Research 33 (1994) 1436–1443.
[37] B.A. Akgun, A.W. Wren, C. Durucan, M.R. Towler, N.P. Mellott, Sol–gel derived silver-incorporated titania thin films on glass: bactericidal and photocatalytic activity, Journal of Sol–Gel Science and Technology 59 (2011) 228–238.